Analytical Decomposition of Nodal Frequency Responses

Jiaxin Wang, *Graduate Student Member, IEEE*, Jiawei Zhang, *Graduate Student Member, IEEE*, Qingchun Hou, *Member, IEEE*, Haiyang Jiang, *Member, IEEE*, Goran Strbac, *Member, IEEE*, Fei Teng, *Senior Member, IEEE*, and Ning Zhang, *Senior Member, IEEE*

***Abstract*—The frequency responses at different buses following a disturbance differ from that of the center-of-inertia (COI). Buses exhibiting much lower frequency nadirs than the COI nadir may pose stability concerns. In this letter, we demonstrate that nodal frequency responses are composed of global and local components. We propose a natural analytical decomposition method to separate these two components. The decomposition provides an insight into the overlap of angle and frequency dynamics. Based on this decomposition, we also derive an indicator that identifies buses susceptible to frequency stability issues. We believe that our findings are fundamental for deepening the understanding of nodal frequency dynamics, with potential applications in related studies. Our work is supported by both numerical simulations and rigorous theoretical analysis.**

***Index Terms*—Angle dynamics, decomposition, IBR, nadir, nodal frequency, regional frequency, RoCoF.**

I. Introduction

FREQUENCY security faces new challenges due to reduced system inertia and inverter-based resource (IBR) penetration. In particular, the variation of frequency responses among buses is a critical challenge. Traditionally, researchers assume that the frequency responses are the same for all buses, and the system frequency is called a global frequency. Various models have been proposed to analyze global frequency dynamics, such as the average system frequency (ASF) model [1], [2] and the common mode frequency (CMF) model [3]. However, the frequency nadirs and arrival times at different buses are not identical. Global frequency models may not reflect these differences.

Failing to consider the variation in nodal frequency dynamics may lead to an underestimation of the severity of frequency issues. Nodal frequency nadirs are usually lower than the center-of-inertia (COI) nadir since the COI frequency is a weighted average of nodal frequencies [4]. Maintaining the COI frequency response within the security limits is insufficient, and the nodal frequency responses should also be considered. An unexpected low nodal frequency may result in disconnections of sensitive loads or even large-scale generators. Meanwhile, the rate of change of frequency (RoCoF) at different buses presents a different pattern from the RoCoF of the COI [5]. We will show in this letter that buses with low frequency nadirs do not necessarily have large RoCoFs. Currently, analyses of nodal frequency dynamics are still not well developed.

This letter finds an natural analytical decomposition for nodal frequency responses. Each nodal frequency response is explicitly decomposed into a global component and a local component. The global component contributes to the frequency of the COI, and the local component reflects the variation of nodal frequency responses. Based on the decomposition, an indicator is proposed to assess the severity of nodal frequency dynamics.

The main contributions of this letter are as follows. 1) We present a natural analytical decomposition method to separate the global and local components of nodal frequency responses. 2) Based on this decomposition, we propose an indicator to assess the severity of nodal frequency dynamics. We would like to highlight the decomposition finding, which is fundamental to understanding nodal frequency dynamics. The decomposition uncovers the interwined relationship between angle and frequency dynamics, where the nodal angle dynamics are reflected in the local component and the global frequency dynamics are captured by the global component.

II. Nodal Frequency Response Model

We introduce a general nodal frequency response model. The model considers the governor dynamics of synchronous generators, the damping effect of loads, the power-frequency loop of IBRs, and the (virtual) inertia/damping of both synchronous generators and IBRs. We use m to represent the (virtual) inertia, d to represent the (virtual) damping coefficients, and μ to represent the load damping coefficients.

Let $\mathcal{G} := \{1, 2, \ldots, n\}$ represent n generation buses and $\mathcal{L} := \{n+1, \ldots, n+n_L\}$ represent n_L load buses. For convenience,

Received 11 May 2024; revised 7 August 2024 and 16 October 2024; accepted 20 October 2024. Date of publication 25 October 2024; date of current version 27 December 2024. This work was supported in part by the National Key R&D Program of China under Grant 2022YFB2403300, in part by the National Natural Science Foundation of China under Grant 52177093, and in part by the Tsinghua University Initiative Scientific Research Program, and Scientific and Technical Project of State Grid Shanghai Electric Power Company under Grant SGSHDK00DWJS2310470. Paper no. PESL-00139-2024. *(Corresponding author: Ning Zhang.)*

Jiaxin Wang, Haiyang Jiang, and Ning Zhang are with the State Key Laboratory of Power Systems, Department of Electrical Engineering, Tsinghua University, Beijing 100084, China (e-mail: jiaxinwangthu@gmail.com; ningzhang@tsinghua.edu.cn).

Jiawei Zhang is with China Electric Power Planning and Engineering Institute Beijing 100120, China.

Qingchun Hou is with the Zhejiang University-University of Illinois Urbana-Champaign Institute Haining 314400, China.

Goran Strbac and Fei Teng are with the Department of Electrical and Electronic Engineering, Imperial College London, SW7 2BU London, U.K..

This article has supplementary material provided by the authors and color versions of one or more figures available at https://doi.org/10.1109/TPWRS.2024.3485951.

Digital Object Identifier 10.1109/TPWRS.2024.3485951

we partition the susceptance matrix B into four blocks according to $\mathcal{G}$ and $\mathcal{L}$ as follows.

$$B = \begin{bmatrix} B_{\mathcal{GG}} & B_{\mathcal{GL}} \\ B_{\mathcal{LG}} & B_{\mathcal{LL}} \end{bmatrix}. \tag{1}$$

The frequency deviation vector (per-unit value), angle deviation vector, and regulated power vector are denoted by ω, θ, and g, respectively. Then, the dynamics related to the (virtual) inertia and damping of the i-th device are as follows.

$$m_i \frac{\mathrm{d}}{\mathrm{d}t}\omega_i + d_i\omega_i = \Delta P_i - P_i^{\text{Net}} + g_i,\ \forall i \in \mathcal{G}, \tag{2}$$

where ΔP_i represents the power disturbance at bus i, and P_i^{Net} represents the power transmitted to bus i from other buses. It should be noticed that the variable P_i^{Net} here is also a deviation value which equals the real value minus the steady-state value, and

$$P_i^{\text{Net}} = e_i^{\mathrm{T}} J\theta + e_i^{\mathrm{T}} L[P_{n+1}^{\text{Net}}, \ldots, P_{n+n_L}^{\text{Net}}]^{\mathrm{T}},\ \forall i \in \mathcal{G}, \tag{3}$$

where e_i is the i-th column of the identity matrix, $J := B_{\mathcal{GG}} - B_{\mathcal{GL}}B_{\mathcal{LL}}^{-1}B_{\mathcal{LG}}$ is the reduced susceptance matrix after eliminating the load buses, and $L := B_{\mathcal{GL}}B_{\mathcal{LL}}^{-1}$ is the load power distribution matrix [4]. The detailed derivation of the above equations can be found in our supplementary [6].

The transfer function of the governor and turbine of synchronous generators is expressed as $G^{p\omega}(s) := -\frac{g(s)}{\omega(s)} = k\frac{\gamma\tau s+1}{\tau s+1}$, where k is the gain coefficient, τ is the time constant, and $\gamma \in (0, 1)$ is the ratio of the faster process. For ease of writing and analyses, the power-frequency loop of IBRs is uniformly expressed as $G^{p\omega}(s) :== -\frac{g(s)}{\omega(s)} = k\frac{1}{\tau s+1}$, which can be viewed as a particular case with $\gamma = 0$. It is worth noting that other expressions of the power-frequency loop may be easily extended to the proposed methods. For example, $G^{p\omega}(s) = k$, $G^{p\omega}(s) = k\frac{1}{s}$, $G^{p\omega}(s) = k_p + k_i\frac{1}{s}$, and even higher-order transfer functions are often used in other studies [3]. We may still integrate these heterogeneous power-frequency loops into a similar time-domain frequency response model and then apply the proposed methods.

We define M as the diagonal matrix composed of m_i, D as the diagonal matrix composed of d_i, K as the diagonal matrix composed of k_i, Γ as the diagonal matrix composed of γ_i, and T as the diagonal matrix composed of τ_i. Then, we give a system-level model based on two widely acceptable assumptions [3], [7]. 1) Neglecting inner loop dynamics: The dynamics of inner loops, such as the current loop of IBRs, are not considered in system-level frequency analysis because they operate on much shorter timescales compared to power-frequency loops. 2) Exclusion of nonlinear blocks: Nonlinear blocks, such as saturation and dead zones, are not accounted for in this letter to facilitate the analysis. As a result, the nodal frequency response model is as follows, and the detailed derivation can be found in our supplementary [6].

$$\frac{\mathrm{d}}{\mathrm{d}t}\begin{bmatrix}\theta\\ \omega\\ g\end{bmatrix} = A\begin{bmatrix}\theta\\ \omega\\ g\end{bmatrix} + \begin{bmatrix}0\\ M^{-1}\\ -N\end{bmatrix}\Delta P, \tag{4}$$

where $N := K\Gamma M^{-1}$,

$$A := \begin{bmatrix} 0 & \omega_0 I_n & 0 \\ -M^{-1}J & -M^{-1}\tilde{D} & M^{-1} \\ NJ & N\tilde{D} - T^{-1}K & -N - T^{-1} \end{bmatrix}, \tag{5}$$

ω_0 is the nominal frequency (usually valued at 50 Hz / 60 Hz), and I_n represents the identity matrix of size n. It is worth noting that ω in this letter represents the frequency deviation, which equals the actual frequency minus the nominal frequency ω_0. In addition, the load damping μ is referred to the generation side by

$$\tilde{D} := D - L\mathrm{diag}(\mu_1, \ldots, \mu_{n_L})F, \tag{6}$$

where $F := -B_{\mathcal{LL}}^{-1}B_{\mathcal{LG}}$ is the coefficient matrix in the frequency divider $[\omega_i]_{i\in\mathcal{L}} = F[\omega_i]_{i\in\mathcal{G}}$ [8], which calculate the load-side frequency deviations using the generation-side frequency deviations. The detailed derivation of the above equations can be found in our supplementary [6].

III. Derivation of the Nodal Frequency Formula

We derive an explicit formula for the nodal frequency responses. A general solution of (4) is given by

$$\omega(t) = [0\ I_n\ 0]\int_0^t \mathrm{e}^{A(t-\tau)}[0\ M^{-1}\ -N]^{\mathrm{T}}\Delta P(t)\mathrm{d}\tau. \tag{7}$$

It should be noticed that the state variables (θ, ω, g) in this letter are all deviations from the steady-state values, and thus the initial conditions are all zeros. From (7), we derive an explicit formula for the nodal frequency responses. For convenience, we write $A = X\mathrm{diag}(\lambda_1, \ldots, \lambda_{3n})X^{-1}$ as the spectral decomposition of A in (4). We define the following three index sets as $\mathcal{I}_0 = \{k \mid \lambda_k = 0\}$, $\mathcal{I}_1 = \{k \mid 0 \neq \lambda_k \in \mathbb{R}\}$, and $\mathcal{I}_2 = \{k \mid \lambda_k \in \mathbb{C} \setminus \mathbb{R}\}$. We use e_j to represent the j-th column of the identity matrix of suitable size.

First, we consider a single disturbance $\Delta P(t) = \Delta P_j e_j \epsilon(t)$ at the generation side, where $\epsilon(t)$ is a step function. The frequency responses are calculated by

$$\begin{aligned}\omega^{(j)}(t) &= [0\ I_n\ 0]X\mathrm{diag}\left(\int_0^t \mathrm{e}^{\lambda_k(t-\tau)}\mathrm{d}\tau\right) \\ &\quad X^{-1}\begin{bmatrix}0 & e_j^{\mathrm{T}} & -k_j\gamma_j e_j^{\mathrm{T}}\end{bmatrix}^{\mathrm{T}} m_j^{-1}\Delta P_j \\ &= \frac{\Delta P_j}{m_j}X_2\mathrm{diag}\left(\frac{\mathrm{e}^{\lambda_k t}-1}{\lambda_k}\right)(\Xi_2 - k_j\gamma_j\Xi_3)\,e_j,\end{aligned} \tag{8}$$

where we write $X_2 := [0\ I_n\ 0]X$, $\Xi_2 := X^{-1}[0\ I_n\ 0]^{\mathrm{T}}$, and $\Xi_3 := X^{-1}[0\,0\,I_n]^{\mathrm{T}}$. According to L'Hôpital's rule, $\lambda_k^{-1}(\mathrm{e}^{\lambda_k t} - 1) = t$ represents a linear term for $k \in \mathcal{I}_0$. In our supplemental material [6], we show that $X_2 e_k = 0$ for $k \in \mathcal{I}_0$, implying that

the linear term in (8) can be removed. Therefore, the frequency response at bus i is simplified as

$$\omega_i^{(j)}(t) = \Delta P_j \sum_{k\notin\mathcal{I}_0} \frac{c_{ijk}}{m_j\lambda_k}(\mathrm{e}^{\lambda_k t}-1),\ \forall i,j\in\mathcal{G} \tag{9}$$

where $c_{ijk} := (e_i^{\mathrm{T}} X_2 e_k)(e_k^{\mathrm{T}}\Xi_2 e_j - k_j\gamma_j e_k^{\mathrm{T}}\Xi_3 e_j)$.

Second, disturbances at the load sides can be analyzed using the superposition principle.

$$\omega_i^{(j)}(t) = \Delta P_j \sum_{k\notin\mathcal{I}_0} \lambda_k^{-1}(\mathrm{e}^{\lambda_k t}-1)\sum_{l\in\mathcal{G}} m_l^{-1} c_{ilk}\ell_{l,j-n}, \tag{10}$$

where $i\in\mathcal{G}$, $j\in\mathcal{L}$, and ℓ_{ij} represent the (i,j) entries of the load power distribution matrix L.

Then, we can obtain the load-side frequency responses via the frequency divider.

$$\omega_i^{(j)}(t) = \begin{cases} \Delta P_j \sum_{k\notin\mathcal{I}_0} \frac{\mathrm{e}^{\lambda_k t}-1}{\lambda_k}\sum_{p\in\mathcal{G}} \frac{f_{i-n,p}c_{pjk}}{m_j}, j\in\mathcal{G} \\ \Delta P_j \sum_{k\notin\mathcal{I}_0} \frac{\mathrm{e}^{\lambda_k t}-1}{\lambda_k}\sum_{p,l\in\mathcal{G}} \frac{f_{i-n,p}c_{plk}\ell_{l,j-n}}{m_l}, j\in\mathcal{L} \end{cases} \tag{11}$$

where $i\in\mathcal{L}$ and f_{ij} represent the (i,j) entries of the frequency divider matrix F [8].

Equation (9)–(11) comprise a complete explicit formula for the nodal frequency responses. Without loss of generality, we focus on (9) in the following analysis. All the results can be extended to (10) and (11) similarly.

Finally, we derive the explicit formula for the RoCoF of the nodal frequency responses from (9).

$$r_{ij}(t) = \frac{\mathrm{d}}{\mathrm{d}t}\omega_i^{(j)}(t) = \Delta P_j \sum_{k=\mathcal{I}_1\cup\mathcal{I}_2} \frac{c_{ijk}}{m_j}\mathrm{e}^{\lambda_k t}. \tag{12}$$

The final value $r_{ij}(\infty)=0$ and the initial value $r_{ij}(0) = \Delta P_j\sum_{k=\mathcal{I}_1\cup\mathcal{I}_2}\frac{c_{ijk}}{m_j} = \Delta P_j e_i^{\mathrm{T}} M^{-1} e_j$, where the last equality is due to $X_2\Xi_2 = I_n$ and $X_2\Xi_3 = 0$.

IV. Decomposition of Nodal Frequency Responses

Every nodal frequency response can be decomposed into two parts according to $\mathcal{I}_1$ and $\mathcal{I}_2$. In supplementary [6], we show $\omega_i^{(j)\prime}(t)$ and $\omega_i^{(j)\prime\prime}(t)$ are real.

$$\omega_i^{(j)}(t) = \omega_i^{(j)\prime}(t) + \omega_i^{(j)\prime\prime}(t), \tag{13a}$$

$$\omega_i^{(j)\prime}(t) = \Delta P_j \sum_{k\in\mathcal{I}_1} \frac{c_{ijk}}{m_j\lambda_k}(\mathrm{e}^{\lambda_k t}-1)\in\mathbb{R}, \tag{13b}$$

$$\omega_i^{(j)\prime\prime}(t) = \Delta P_j \sum_{k\in\mathcal{I}_2} \frac{c_{ijk}}{m_j\lambda_k}(\mathrm{e}^{\lambda_k t}-1)\in\mathbb{R}. \tag{13c}$$

The decomposition in (13) shows that the nodal frequency response can be naturally divided into two components. The global component $\omega_i^{(j)\prime}(t)$, a summation of exponential functions, reflects the trend of the COI frequency. The local component $\omega_i^{(j)\prime\prime}(t)$, a summation of decaying trigonometric functions, manifests the inherent traits of local frequency. Theorem 1 reveals that the COI frequency $\widehat{\omega^{(j)}}(t)$ is mainly driven by the global component. We use $\mathrm{tr}M$ to denote the trace of the matrix M, then

$$\widehat{\omega^{(j)}}(t) := \frac{1^{\mathrm{T}}M\omega^{(j)}(t)}{\mathrm{tr}M} \approx \frac{1^{\mathrm{T}}M\omega^{(j)\prime}(t)}{\mathrm{tr}M}. \tag{14}$$

The typical value of the upper bound in (15) is approximately 5×10^{-6} Hz/MW in our test system. We also note that the upper bound is a rough estimation in theory. The inequality cannot hold with strict equality, and the actual contribution of the local component to the COI frequency is even less siginificant, as discussed in Section VI. Therefore, the local component mainly reflects the difference between the nodal frequency response and the COI frequency response.

Theorem 1: The average of $\omega_i^{(j)\prime\prime}(t)$ weighted by the inertia m_i on bus $i=1,2,\ldots,n$ is bounded according to

$$\left|\frac{1^{\mathrm{T}}M\omega^{(j)\prime\prime}(t)}{\mathrm{tr}M}\right| < |\Delta P_j|\frac{2\|1^{\mathrm{T}}MX_2''\|\|(\Xi_2''-k_j\gamma_j\Xi_3'')e_j\|}{m_j\mathrm{tr}M\min_{k\in\mathcal{I}_2}|\lambda_k|}. \tag{15}$$

X_2'' is the columns of X_2 corresponding to $\mathcal{I}_2$, and Ξ_2'', Ξ_3'' are the rows of Ξ_2, Ξ_3 corresponding to $\mathcal{I}_2$, respectively.

Proof: See our supplemental material [6] for details. □

V. Indicator of Nodal Frequency Variations

The analysis in Section IV suggests that the COI frequency is driven by the global component $\omega^{(j)\prime}(t)$. By contrast, the difference between the nodal frequency and the COI frequency is driven by the local component $\omega^{(j)\prime\prime}(t)$. The local component can be viewed as a combination in a function space spanned by $\mathrm{e}^{\lambda_k t}$ for $k\in\mathcal{I}_2$. The coefficient $m_j^{-1}\lambda_k^{-1}c_{ijk}$ measures the amplitude of the k-th basis function. The nodal frequency variations can be measured by the following norm.

$$s_{ij} := \left\|\left[\frac{c_{ijk}}{m_j\lambda_k}\right]_{k\in\mathcal{I}_2}\right\|\quad i,j=1,2,\ldots,n. \tag{16}$$

s_{ij} indicates the severity of the nodal frequency at bus i when a disturbance occurs at bus j. A larger s_{ij} implies a more severe nodal frequency variations.

VI. Case Studies

A modified IEEE 118-bus system is used as the test system. Fifty-four generators are connected to 118 load buses through transformers. A 1200 MW disturbance is applied at load bus #50. The codes in this section are written in Python 3.10, and the computations are performed on an AMD-RT-5950X CPU.

First, we verify the accuracy of the proposed decomposition and the associated theoretical analysis in Section IV. In Fig. 1, we depict the frequency of the COI by dividing it into two components via the decomposition (13). The results indicate that the frequency of the COI is primarily governed by $\omega^{(j)\prime}(t)$. The component $\frac{1^{\mathrm{T}}M\omega^{(j)\prime\prime}(t)}{\mathrm{tr}M}$ of the COI frequency is three orders of magnitude smaller than the component $\frac{1^{\mathrm{T}}M\omega^{(j)\prime}(t)}{\mathrm{tr}M}$. The contribution of $\omega^{(j)\prime\prime}(t)$ is less than 0.3%, rendering it practically negligible. Therefore, the numerical findings align with the theoretical analysis in Section IV. The global component $\omega^{(j)\prime}(t)$ is the primary contributor to the COI frequency, while the local

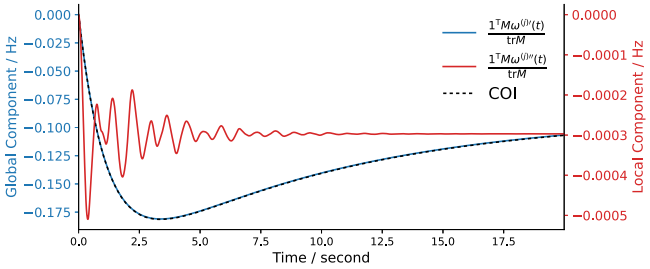

Fig. 1. Components of the COI frequency. The blue and red lines represent global and local components, respectively.

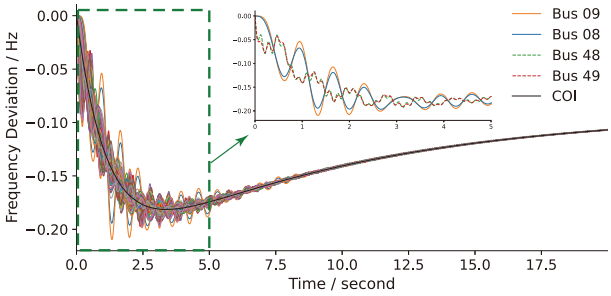

Fig. 2. Variations in spatial frequency responses.

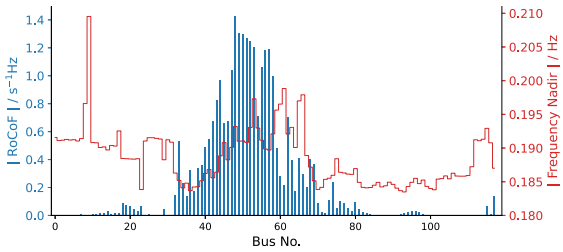

Fig. 3. Blue bars represent the initial RoCoF across all load buses. The red line represents the frequency nadirs.

component $\omega^{(j)\prime\prime}(t)$ is the primary contributor to the variations in the nodal frequencies.

Then, we present the variations in nodal frequency responses. As depicted in Fig. 2, the frequency nadirs vary across different buses. This variations is not captured in the frequency of COI. Traditionally, the frequency nadir and the initial RoCoF are found to be directly correlated in the analysis of the COI frequency. However, this relationship does not hold when analyzing the nodal frequency responses. Fig. 3 shows the initial RoCoF at all load buses. Notably, buses #48 and #49 exhibit the two highest RoCoFs. However, in the subfigure of Fig. 2, it is evident that buses #48 and #49 display better frequency nadirs than buses #09 and #08. By contrast, the RoCoFs at buses #09 and #08 are negligible. The RoCoFs and frequency nadirs present very different patterns when analyzing nodal frequencies.

Finally, we verify the effectiveness of our proposed indicator s_{ij}. Fig. 4 shows the values of s_{ij} across all load buses. A high s_{ij}

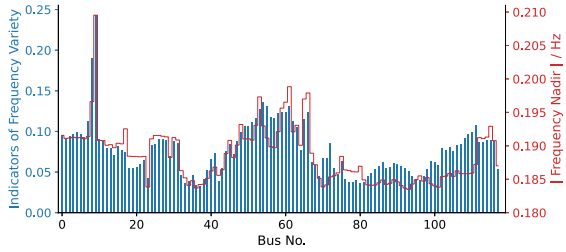

Fig. 4. Blue bars represent our proposed indicator s_{ij} across all load buses. The red line represents the frequency nadirs.

value indicates significant nodal frequency variation. Notably, buses #09 and #08 exhibit the two highest s_{ij} values, corroborating their status as the most severe buses, as demonstrated in the subfigure of Fig. 2.

VII. Conclusion

This letter proposes a natural decomposition for nodal frequency responses. The nodal frequency at each bus can be decomposed into global and local components. The global component contributes to the COI frequency, while the local component reflects the difference between the nodal frequency and the COI frequency. The decomposition provides an insight into the overlap of angle and frequency dynamics, which is essential for understanding nodal frequency responses. Additionally, our analyses and findings may be valuable for other related studies. For instance, they may aid in identifying weak buses, labeling related data for machine learning models, quickly excluding infeasible operation solutions, designing frequency control strategies, adjusting controllable parameters, modeling frequency-security constraints, etc.

References

[1] M. L. Chan, R. D. Dunlop, and F. Schweppe, "Dynamic equivalents for average system frequency behavior following major distribances," *IEEE Trans. Power App. Syst.*, vol. PAS-91, no. 4, pp. 1637–1642, Jul. 1972.

[2] Q. Shi, F. Li, and H. Cui, "Analytical method to aggregate multi-machine SFR model with applications in power system dynamic studies," *IEEE Trans. Power Syst.*, vol. 33, no. 6, pp. 6355–6367, Nov. 2018.

[3] H. Gao et al., "Common-mode frequency in converter-integrated power systems: Definition, analysis, and quantitative evaluation," *IEEE Trans. Power Syst.*, vol. 37, no. 6, pp. 4846–4860, Nov. 2022.

[4] J. Zhang, J. Wang, N. Zhang, P. Wang, Y. Wang, and C. Fang, "Droop coefficient placements for grid-side energy storage considering nodal frequency constraints under large disturbances," *Appl. Energy*, vol. 357, 2024, Art. no. 122444.

[5] M. Tuo and X. Li, "Security-constrained unit commitment considering locational frequency stability in low-inertia power grids," *IEEE Trans. Power Syst.*, vol. 38, no. 5, pp. 4134–4147, Sep. 2023.

[6] J. Wang et al., "Supplemental material for analytical decomposition of nodal frequency responses," 2024. [Online]. Available: https://drive.google.com/drive/folders/1YXDgti2FK4u28OwBwwxSf_2mlipL6tCM?usp=drive_link

[7] J. Chen, M. Liu, and F. Milano, "Aggregated model of virtual power plants for transient frequency and voltage stability analysis," *IEEE Trans. Power Syst.*, vol. 36, no. 5, pp. 4366–4375, Sep. 2021.

[8] F. Milano and A. Ortega, "Frequency divider," *IEEE Trans. Power Syst.*, vol. 32, no. 2, pp. 1493–1501, Mar. 2017.